Green Fluorescent Protein Ground States: The Influence of a Second Protonation Site near the Chromophore[†,‡]

Ranieri Bizzarri,[*,§,||] Riccardo Nifosì,[||] Stefania Abbruzzetti,[⊥] Walter Rocchia,[§] Sara Guidi,[§] Daniele Arosio,[||] Gianpiero Garau,[#] Barbara Campanini,[▽] Elena Grandi,[⊥] Fernanda Ricci,[§] Cristiano Viappiani,[⊥] and Fabio Beltram[§,||]

Scuola Normale Superiore−IIT Research Unit, Piazza dei Cavalieri 7 I-56126 Pisa, Italy, Scuola Normale Superiore−NEST CNR-INFM, Via della Faggiola 19, I-56126 Pisa, Italy, Dipartimento di Fisica, Università di Parma−NEST CNR-INFM, Viale G. P. Usberti 7A, 43100 Parma, Italy, Dipartimento di Biochimica e Biologia Molecolare, Università di Parma, Viale G. P. Usberti 23A, 43100 Parma, Italy, and Biocrystallographic Unit−DIBIT, San Raffaele Scientific Institute, Via Olgettina 56, 20134 Milano, Italy

Received December 26, 2006; Revised Manuscript Received February 26, 2007

ABSTRACT: The photophysical properties of most green fluorescent protein mutants (GFPs) are strongly affected by pH. This effect must be carefully taken into account when using GFPs as fluorescent probes or indicators. Usually, the pH-dependence of GFPs is rationalized on the basis of the ionization equilibrium of the chromophore phenol group. Yet many different mutants show spectral behavior that cannot be explained by ionization of this group alone. In this study, we propose a general model of protonation comprising two ionization sites (2S model). Steady-state optical measurements at different pH and temperature and pH-jump relaxation experiments were combined to highlight the thermodynamic and kinetic properties of paradigmatically different GFP variants. Our experiments support the 2S model. For the case of mutants in which E222 is the second protonation site, thermodynamic coupling between this residue's and the chromophore's ionization reactions was demonstrated. In agreement with the 2S model predictions, X-ray analysis of one of these mutants showed the presence of two chromophore populations at high pH.

Green fluorescent protein (GFP[1]) and its homologues are powerful research tools in molecular and cell biology (*1*). The GFP chromophore is autocatalytically generated by a multistep chemical reaction of a 3-amino acid sequence (S65-Y66-G67) and is characterized by a 4-hydroxybenzylidene imidazolinone structure conjugated to a phenol ring (*2*). The proper arrangement of the other residues in a compact 11-stranded β-barrel enveloping the chromophore is a prerequisite for fluorescence, since the isolated chromophore is not fluorescent in aqueous solution at room temperature (RT[1]) (*3*). Modification of the original GFP (wtGFP) primary sequence mostly by means of random mutation and library screening yielded artificial fluorescent proteins with tuned excitation and emission wavelengths, improved photophysical characteristics, and sensitivity to modifications of the intracellular environment (*1*, *4*). Experimental analyses and theoretical calculations, however, have only partially unraveled the interplay between structure dynamics and spectral events in GFPs (*5*, *6*, *7*).

The absorption spectrum of wtGFP contains two main bands in the visible region, centered at about 395 and 475 nm, which were attributed to neutral (named A state) and anionic (named B state) forms of the chromophore, respectively (*8*). The almost identical emission spectra of A and B originate from a common emission pathway from the excited anionic chromophore. This is mediated by an excited-state proton transfer (ESPT[1]) mechanism that involves one or more metastable states where the protein conformation is not relaxed (*5*, *9*, *10*).

Most GFP variants display optical properties fairly dependent on pH in the physiological range (*11*−*14*), and the observed phenomenology is largely consistent with the idea that only chromophore ionization affects the protein optical properties at equilibrium. There exists experimental evidence, however, that can hardly be explained on the basis of this hypothesis. Most relevant is the large absorption of the neutral chromophore at proton concentrations much lower than the apparent dissociation constant observed for many mutants such as T203V, deGFPs (base mutations: S65T/T203C), Sapphire/H9 (S202F/T203I), and RaGFP (complex

[†] This work was partially supported by Fondazione Monte dei Paschi, Siena, Italy, and the Italian Ministry of University and Scientific Research under FIRB RBLA03ER38.

[‡] Structural data for E[2]GFP were deposited in the Protein Data Bank using accession code 2H9W.

* To whom correspondence should be addressed. E-mail: r.bizzarri@sns.it. Tel: +39 050 509434. Fax: +39 050 509417.

[§] Scuola Normale Superiore−IIT Research Unit, Pisa.

[||] Scuola Normale Superiore−NEST, CNR-INFM.

[⊥] Dipartimento di Fisica, Università di Parma−NEST CNR-INFM.

[#] Biocrystallographic Unit−DIBIT, San Raffaele Scientific Institute.

[▽] Dipartimento di Biochimica e Biologia Molecolare, Università di Parma.

[1] Abbreviations: GFP, green fluorescent protein; RT, room temperature; wtGFP, wild type green fluorescent protein; ESPT, excited-state proton transfer; 2S, two-site protonation model; XH, second protonation site near the chromophore; ChroH, chromophore phenol group; E[n]GFPs, enhanced green fluorescent protein family; EGFP, F64L/S65T GFP; E[1]GFP, F64L/T203Y GFP; E[2]GFP, F64L/S65T/T203Y GFP; Mut2s, Mut2 protein family; Mut2V, T203V Mut2; Mut2Y, T203Y Mut2; Mut2G, H148G Mut2; ACA, augmented component analysis; FCS, fluorescence correlation spectroscopy.

10.1021/bi602646r CCC: $37.00
Published on Web 04/17/2007

mutation pattern) (*14*−*17*). One could postulate the presence of a chromophore fraction kinetically "frozen" in the neutral ground state, whose absorption band simply adds up to the spectrum of the ionizable fraction of the chromophore. This hypothesis, however, is questioned by the available X-ray structures of some representative variants at high pH. These data seem to exclude the concomitant presence of two distinguishable three-dimensional configurations of the chromophore environment (*14*). The presence of a frozen fraction of protonated chromophore seems also unlikely according to the results of a recent study, which reported reversible shifts between the anionic and neutral absorption bands in some deGFP variants by changing the temperature at high pH (*18*). Note that the residual presence of a protonated chromophore fraction at high pH may have significant consequences for several biophysical applications of GFPs. For instance, the presence of a sizable neutral band in the spectrum of F64L/S65T/T203Y was exploited by us to develop a new excitation and emission intracellular pH indicator tailored for the 6−8 pH range (*19*).

In this study, we propose an alternative 2-site protonation model (2S model) that can explain all the observed spectral features and overcome the shortcomings of the simple ionization scheme adopted so far. The new model takes into account the presence of a second ionizable group (XH^1) near the chromophore whose protonation equilibrium can be *thermodynamically coupled* in an anti-cooperative fashion with that of the phenol in the chromophore (hereafter denoted as $ChroH^1$) owing to the high repulsive energy of two negatively charged groups located in close proximity. The 2S model represents a generalization of the single chromophore ionization scheme, to which it reduces when XH is not thermodynamically coupled to ChroH.

In this work, we shall provide experimental evidence to support the applicability of the 2S model to describe the optical properties of GFP mutants by a combined thermodynamic and kinetic approach. In particular, we focus here our attention on two GFP families, which will be shown to represent distinct paradigms of ground-state protonation patterns. The first family (E^nGFPs^1) is constituted by the popular "enhanced" green fluorescent protein (EGFP, F64L/S65T GFP^1) (*20*) and two closely related variants (E^1GFP, F64L/T203Y GFP^1; E^2GFP, F64L/S65T/T203Y GFP^1). The second family ($Mut2s^1$) is constituted by the Mut2 protein (Mut2, S65A/V68L/S72A GFP^1) (*21*), and three variants sharing its base mutation pattern but adding a further amino acid replacement compared to GFP (Mut2V, T203V $Mut2^1$; Mut2Y, T203Y $Mut2^1$; Mut2G, H148G $Mut2^1$). Note that, in search of a general approach, we considered mutations in the primary sequence which are reported to strongly influence the optical properties of GFPs (*1*, *15*, *16*) while still preserving the ionization equilibrium of the chromophore.

Finally, we shall show that E^nGFPs display anti-cooperative coupling between ChroH and XH, while this does not happen for Mut2s, and we shall link this different behavior to the nature of the XH residue and mutation pattern.

EXPERIMENTAL PROCEDURES

All inorganic and organic materials (buffer components, stabilizers, and indicators) were purchased from Sigma-Aldrich.

Plasmid Construction, Protein Expression, and Purification. The construction of the protein codifying plasmids and their bacterial expression, purification, and characterization were carried out according to previously published procedures (*19*, *22*). The molar concentrations of the proteins in the folded form were determined according to the method of Ward (*20*).

Spectroscopic Measurements. Absorption and fluorescence spectra were recorded at 23 °C on a Jasco V550 spectrophotometer (Jasco, Easton, MD) or a Cary Eclipse spectrofluorometer (Varian, Palo Alto, CA), adopting the collection parameters reported in ref *19*. From the molar concentrations of the proteins, we calculated the following extinction coefficients (M^{-1} cm^{-1}) at 278 nm (ϵ_{UV}): EGFP, 32 650; E^1GFP, 31 350; E^2GFP, 31 140; Mut2, 31 560; Mut2V, 30 970; Mut2Y, 36 040; Mut2G, 29 805. For the thermal analysis, absorption spectra of the protein mutants were collected at pH 9.0 (buffer: 20 mM diethanolamine) every 3−5 K from 293 to 330 K. The related mathematical treatment is reported in the Supporting Information.

Acid−*Base Titrations and Optical Data Analysis.* Titrations of absorbance and fluorescence versus pH were performed on 2.0 μM protein samples dissolved in a citrate−phosphate (2−10 mM) buffer whose pH was adjusted to the desired value by addition of 1 M NaOH. Data were analyzed by means of the augmented component analysis (ACA^1) method, whose characteristics are reported as the Supporting Information.

Kinetic Relaxation Measurements. Photoexcitation of the caged proton compound 2-nitrobenzaldehyde (2-NBA) was carried out with the third harmonic (355 nm) of a Q-switched Nd:YAG laser (Continuum, Santa Clara, CA). The 488 nm (EGFP) or 514 nm (E^1GFP, E^2GFP, and Mut2Y) line of an Ar^+ laser (Uniphase, San Jose, CA) was used as probe source for transient absorption signals or excitation source for transient fluorescence signals. Measurements were performed at different UV-laser pulse energies (5−40 mJ). The concentration of photoreleased protons was calibrated by recording the protonation kinetics of a pH indicator. In the reported experiments $[H^+]$ varied between about 39 μM (5 mJ laser pulse energy) and 210 μM (40 mJ laser pulse energy), while the protein concentration was kept in the 0.2−0.8 μM range. The kinetic events upon the photorelease of H^+ ions were followed by observing the change of both the absorbance at the wavelength of the probe laser and the fluorescence emission excited by the same laser beam. Nonetheless, the higher S/N ratio of the transient fluorescent signals made them the favorite traces for the kinetic data analysis. Optical changes occurred in the micro- to millisecond time scale and were investigated as a function of the pH-jump (i.e., of laser pulse energy). Changes in absorption and fluorescence emission became faster as the concentration of photoreleased H^+ was increased, indicating that they were associated with the change in pH of the solution. Control experiments allowed the attribution of the optical signals specifically to the protein protonation. Indeed, an error source in the determination of ionization kinetics might be represented by photoactivation, as illumination of wtGFP and other mutants with high-power UV/vis light triggers E222 decarboxylation, with a parallel increase of the anionic chromophore B band at 483 nm (*23*). Furthermore, a photoconversion process of previously photobleached molecules upon illumination at

Scheme 1: Representation of the Protonation Equilibria of the 2S Model[a]

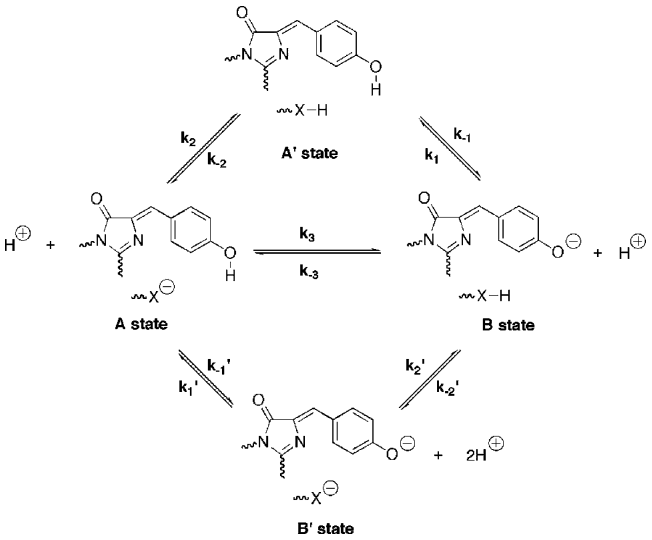

[a] Wavy lines are supposed to connect chromophore and the XH group to the protein sequence. In evidence are reported the microscopic rate constants for each protonation reaction. The equilibrium constants for these reactions are expressed as follows: $K_{A'A} = k_{-2}/k_2 = [A][H^+]/[A']$; $K_{A'B} = k_{-1}/k_1 = [B][H^+]/[A']$; $K_{AB} = k_3/k_{-3} = [B]/[A]$; $K_{BB'} = k_{-2}'/k_2' = [B'][H^+]/[B]$; $K_{AB'} = k_{-1}'/k_1' = [B'][H^+]/[A]$.

350 nm has been demonstrated for E^{2}GFP (*24*, *25*). Accordingly, we evaluated transient absorption spectra of E^{2}GFP before and after a single excitation pulse at 355 nm, demonstrating that they were absolutely identical and no photoactivation processes took place at the typical laser powers of our setup.

Data were analyzed by considering the protonation equilibria of the 2S model (Scheme 1) together with the reactions of all the other ionizable residues in the protein organized into two general classes (COOH and His), following the approach and symbology reported in ref *22*. The differential equations describing the ionization equilibria were solved by using the function ODE15s of Matlab. The equation parameters (rate constants, initial concentration, and p*K* values) were optimized using a nonlinear fitting algorithm (package Minuit, CERN). Significantly, a global analysis was performed on experimental curves at different pump laser pulse energies.

Crystallography. Polyhistidine tag-free E^{2}GFP were grown at 20 °C in 1−2 weeks, mixing 2 μL of protein solution (15 mg/mL) with 2 μL of well solution containing 1.8 M ammonium sulfate and 100 mM Tris pH 9.0. At 289 K, E^2-GFP crystal diffracted to 1.8 Å resolution at the ESFR beamline BM30A. The intensities of diffraction patterns were integrated with MOSFLM (*26*) and scaled with SCALA from CCP4 packages. Molecular replacement was performed using MOLREP (CCP4), with the protein atoms of 2H6V structure as starting model. The chromophore atoms were modeled in the map after most of the protein and water molecules were built and refined. Conformational torsion angle, restraints, and charge assignments for the chromophore were obtained using CCP4i Libcheck. The structure was refined using REFMAC (CCP4). Data collection parameters and refinement statistics are reported in the Supporting Information. Coordinates and structure factors have been deposited in the Protein Data Bank using accession code 2H9W.

RESULTS

Two-Site Protonation Model (2S Model). Scheme 1 displays the protonation model adopted to describe the ground state equilibria affecting the optical properties of the GFP mutants. Two ionizable sites are of relevance: the phenol in the chromophore (ChroH) and a group (XH) in the immediate surroundings, yielding four communicating ground states (A′, A, B, and B′). Internal and external proton transfer can be either direct or mediated by other residues and/or water molecules. Only the thermodynamically stable conformational forms of the chromophore and its environment are considered. The inclusion of intermediate/metastable species would not change the description of the protonation equilibria.

The microstate approach of Ullmann (*27*) provides a convenient framework to describe mathematically the population of the four states, by using the notation of Scheme 1. The protein molar absorbance (Abs) is given by the sum of each molar fraction multiplied by the molar extinction coefficient (ϵ) of the related state. We can write

$$\mathrm{Abs}(\lambda) = [\epsilon_{A'}(\lambda) + \epsilon_A(\lambda) \times 10^{(\mathrm{pH}-\mathrm{p}K_{A'A})} + \epsilon_B(\lambda) \times 10^{(\mathrm{pH}-\mathrm{p}K_{A'B})} + \epsilon_{B'}(\lambda) \times 10^{(2\mathrm{pH}-\mathrm{p}K_{A'A}-\mathrm{p}K_{A'B}-W)}] \times [1 + 10^{(\mathrm{pH}-\mathrm{p}K_{A'A})} + 10^{(\mathrm{pH}-\mathrm{p}K_{A'B})} + 10^{(2\mathrm{pH}-\mathrm{p}K_{A'A}-\mathrm{p}K_{A'B}-W)}]^{-1} \quad (1)$$

where W is proportional to the interaction free energy between the ionization sites. We consider only positive W values; that is, the release of the first proton from any of the two sites hinders the release of the second (negative cooperativity) because of electrostatic repulsion. If the four states have pH-independent quantum yields, eq 1 with ϵ replaced by $\epsilon\Phi$ describes also the fluorescence emission. Two cases are of relevance for the description of GFP optical properties:

(1) $W = 0$: ChroH and XH Residue Are Not Thermodynamically Coupled. Under the reasonable hypothesis that the two residues are optically independent ($\epsilon_A \approx \epsilon_{A'}$ and $\epsilon_B \approx \epsilon_{B'}$), eq 1 becomes

$$\mathrm{Abs}(\lambda) = \frac{[\epsilon_{A'}(\lambda) + \epsilon_B(\lambda) \times 10^{(\mathrm{pH}-\mathrm{p}K_{A'B})}]}{1 + 10^{(\mathrm{pH}-\mathrm{p}K_{A'B})}} \quad (2)$$

Thus, the optical response of the protein upon pH follows the single ionization equilibrium of ChroH.

(2) $W \gg 0$: ChroH and the XH Residue Are Strongly Thermodynamically Coupled. Here, we neglect the optical contribution of the B′ state, as it becomes significantly populated only at pH $\approx [(\mathrm{p}K_{A'A} + \mathrm{p}K_{A'B} + W)/2]$, supposedly well beyond the pH stability range of the protein. In addition, we introduce

$$K_{A'M} = K_{A'A} + K_{A'B} = K_{A'A}(1 + K_{AB}); \quad \epsilon_M = \frac{\epsilon_A + \epsilon_B K_{AB}}{1 + K_{AB}} \quad (3)$$

Scheme 2 [a]

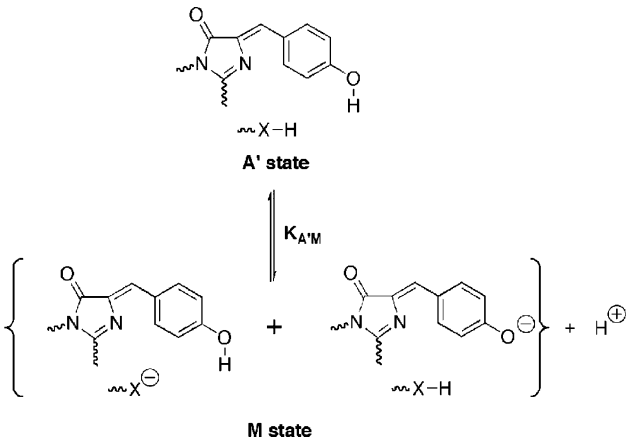

[a] For strongly coupled ChroH and XH, the B′ state may be not appreciably populated before the unfolding pH of the protein. In such a case, the protein optical properties follow a two-state equilibrium between the fully protonated form A′ and an apparent form M. $[M] = ([A] + K_{AB}[B])/(1 + K_{AB})$. $K_{A'M} = [M][H^+]/[A']$.

Thus, we obtain from eq 1

$$\mathrm{Abs}(\lambda) = \frac{[\epsilon_{A'}(\lambda) + \epsilon_M(\lambda) \times 10^{(\mathrm{pH}-\mathrm{p}K_{A'M})}]}{1 + 10^{(\mathrm{pH}-\mathrm{p}K_{A'M})}} \qquad (4)$$

Equation 4 describes the signal due to the ionization between A′ and the *apparent* ground state M, composed of a mixture of A and B states (Scheme 2). $K_{A'M}$ is the dissociation constant and ϵ_M is the molar extinction coefficient (M^{-1} cm^{-1}) of M. Thus, when the two sites are strongly coupled, the optical response *is still described by a single-site equation*. Equation 4 shows that, for comparable molar extinction coefficients of A and B ($\epsilon_A \sim \epsilon_B$), and K_{AB} not too different from unity, the protein would show some absorption and/or fluorescence due to the neutral chromophore even at high pH.

Noticeably, eqs 2 and 4 are formally identical; however, eq 4 has a much more general value (and will be used in the following sections), as the uncoupled protonation pattern may be seen as a special case of the A′ ↔ M equilibrium for which state M merges with B.

pH-Dependent Photophysical Properties. Steady-state absorption measurements showed that all mutants had a pH-dependent absorption spectrum in the visible region, characterized by two peaks attributable to neutral (391−423 nm) and anionic chromophore (476−515 nm) (as exemplified for E^2GFP in Figure 1). At pH above 10−11, the protein unfolds and the absorption spectrum showed the 448-peaked band typical of the chromopeptide in basic solution (*28*). The low-energy band increased from zero to an asymptotic value as pH was raised, while the high-energy band followed the opposite trend (not shown). For all mutants, a clearly defined isosbestic point in the absorption spectra suggested the existence of a single protonation equilibrium.

The protein steady-state absorption and fluorescence spectra were globally fitted to eq 4 by means of a developed ad hoc algorithm (ACA) conceptually similar to principal component analysis (see Supporting Information). Convergence of the fitting algorithm yielded $pK_{A'M}$ (Table 1) and the molar spectral responses of states A′ and M for each protein (Figure 2). No simple correlation of $pK_{A'M}$ with the protein mutation pattern was recognized, although the rather high $pK_{A'M}$ of Mut2G is similar to the pK_a values reported in literature for other H148G variants (*13*, *29*). Table 2 lists the wavelengths of absorption maxima and the associated extinction coefficients.

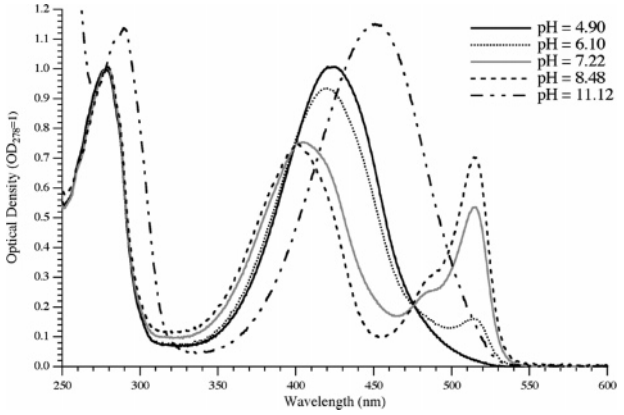

FIGURE 1: Molar absorption spectra of E^2GFP taken at different pHs.

The maximum absorption wavelength of the A′ state is located around 390−396 nm for most mutants (Figure 2, left), a value nearly identical to that reported for wtGFP (397 nm) (*5*). E^1GFP, E^2GFP, and Mut2Y represent exceptions to this behavior, as they showed maxima in the 410−423 nm interval.

At high pH, E^1GFP and E^2GFP show a large absorption due to the neutral chromophore around 400 nm, whose intensity did not change by further increasing pH (not shown). Conversely, the other mutants are characterized by small bands or shoulders in the same spectral region. Under the framework of the 2S model, we attributed this band to the optical contribution of the A state to the M mixed state (Figure 2). Absorption of the B state peaked at 476−489 nm for EGFP, Mut2, Mut2G and was significantly red-shifted for the other mutants (Figure 2, right). As expected (*14*, *15*, *30*), the largest red-shifts were shown by the three T203Y variants E^1GFP, E^2GFP, and Mut2Y, with absorption maxima at 509−515 nm.

The fluorescence excitation spectra of the proteins were found to be similar to the corresponding absorption spectra at both low and high pH (not shown). This observation suggests distinguishable excitation/emission pathways for the three protonation ground states, each one characterized by a relatively pH-independent fluorescence quantum yield. Accordingly, the $pK_{A'M}$ values calculated from fluorescence excitation/emission spectra were very close to those obtained by absorption, with the exception of Mut2G, whose fluorescence p*K* resulted 0.2 unit lower. Regardless of the ground state, the major emission band was always in the green-yellow region of the spectrum (508−523 nm). The introduction of Y203 led to 10−12 nm emission red-shift of the anionic chromophore, in agreement with the reported fluorescence characteristics of other T203Y variants (*15*, *30*).

Temperature Dependence of the Optical Properties at High pH. According to the 2S model in the case of mutants characterized by coupled ChroH and XH only the proton transfer between the A and B states is active at high pH ($> pK + 2$). The two states cannot be optically distinguished by changing pH (as they constitute the pH-independent M

Table 1: Ionization p*K* Values and Kinetic Rate Constants Calculated by Steady-State (eq) and Kinetic Relaxation (kin) Optical Measurements[a]

parameter	EGFP	E^{1}GFP	E^{2}GFP	Mut2	Mut2V	Mut2Y	Mut2G
p$K_{A'M}$ (eq)	5.85	6.00	6.78	5.70	6.18	6.26	7.41
p$K_{A'B}$ (eq)	5.92	7.20	7.29	5.70	6.18	6.26	7.41
p$K_{A'B}$ (kin)	5.90	7.25	7.29	*6.12*	*6.21*	6.30	*7.57*
p$K_{A'A}$ (eq)	6.65	6.03	6.94	nd	nd	nd	nd
p$K_{A'A}$ (kin)	6.70	6.09	6.90	*5.35*	*5.40*	5.34	*nd*
k_1[b] (Chro$^-$ + H$^+$)	3.6	3.5	4.0	*0.1*	*0.01*	3.6	*30*
k_2[c] (X$^-$ + H$^+$)	5.0	5.5	5.5	*5.0*	*5.0*	5.5	*nd*
k_{-3}[c] (XH + Chro$^-$)	<0.03	4.0	0.56	*29*	*13*	36.5	*nd*
k_4[d] (RCOO$^-$ + H$^+$)	5.41	5.38	5.35	*5.40*	*5.40*	5.33	*5.40*
k_{-5}[e] (RCOOH + Chro$^-$)	0.12	1.9	2.25	*4.0*	*4.0*	0.32	*18.0*
k_6[c] (RCOOH + X$^-$)[h]	1.0	1.0	1.4	*1.0*	*1.0*	1.2	*nd*
k_7[c] (His + H$^+$)	5.9	6.3	6.3	*6.3*	*6.2*	6.2	5.5
k_8[b] (HHis$^+$ + X$^-$)[h]	8.6	8.6	8.6	*8.5*	*8.6*	8.6	*nd*
k_9[f] (HHis$^+$ + Chro$^-$)[h]	90000	170	200	*0.61*	*13*	150	0.09
k_{-10}[c] (His + RCOOH)[h]	1.04	1.04	1.04	*1.0*	*1.0*	1.04	1.1
k_c[g]	0.8	nd	nd	*1.2*	*0.45*	nd	*0.93*

[a] The previously determined kinetic parameters of Mut2, Mut2V, and Mut2G (*22*) are tabulated in italics for comparison. nd = not determined. [b] 10^7 M^{-1} s^{-1}. [c] 10^9 M^{-1} s^{-1}. [d] 10^{10} M^{-1} s^{-1}. [e] 10^8 $M^{-1}s^{-1}$. [f] 10^3 M^{-1} s^{-1}. [g] 10^3 s^{-1}. [h] Very little dependence on these parameters was observed, although their value is indicative of a low exchange rate.

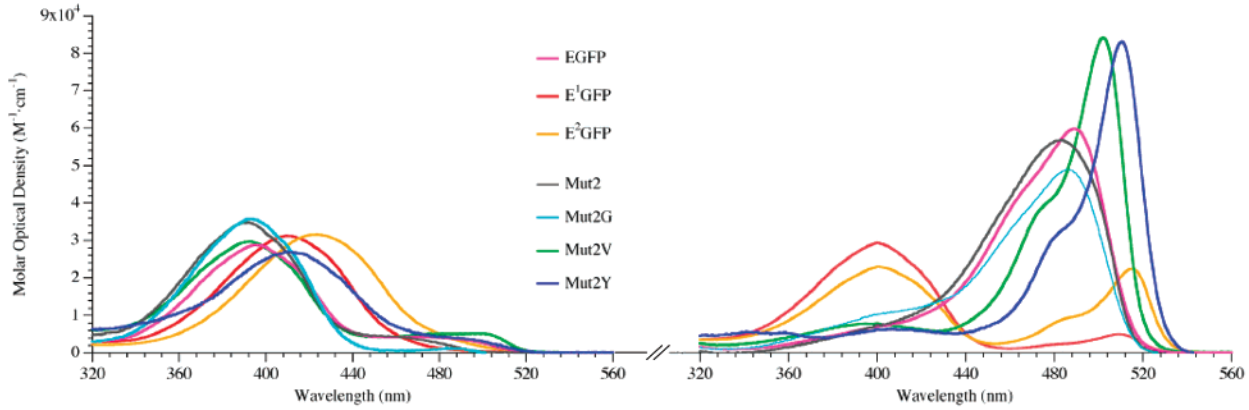

FIGURE 2: Molar absorption spectra of A′ state (left panel) and M state (right panel).

Table 2: Protein Absorption Wavelengths and Extinction Coefficients Determined by ACA[a]

protein	$\lambda_{A'}$ (nm)	$\epsilon_{A'} \times 10^4$ (M^{-1} cm^{-1})	λ_A (nm)	$\epsilon_A \times 10^4$ (M^{-1} cm^{-1})	λ_B (nm)	$\epsilon_B \times 10^4$ (M^{-1} cm^{-1})
EGFP	396	2.87	400(s)	nd	489	5.95
E^{1}GFP	410	3.13	400	2.93	509	0.50
E^{2}GFP	423	3.16	401	2.28	515	2.22
Mut2	390	3.15	398(s)	nd	483	5.78
Mut2V	392	2.96	397	0.78	502	8.39
Mut2Y	411	2.69	406	0.63	510	8.27
Mut2G	393	3.57	402(s)	nd	486	4.88

[a] $\lambda_{A'}$, λ_A, and λ_B: wavelengths at maximum of the A′, A, and B absorption bands. nd = not detected.

form). This may be accomplished by changing the temperature if the A ↔ B interconversion is associated with a nonvanishing ΔH_{AB}. We found that only E^{n}GFPs were characterized by a significant thermal dependence of their A ↔ B equilibrium. E^{1}GFP and E^{2}GFP showed an increase of the B band and a decrease of the A band with the temperature (Figure 3), whereas EGFP displayed the opposite behavior. The presence of a clear isosbestic point supported our hypothesis of a temperature-dependent equilibrium between two states whose optical properties are unchanged by pH.

Considering two spectral regions λ_1 and λ_2 where A and B do not show appreciable absorption overlap, and assuming that the extinction coefficients of A and B are not modified by temperature, the relations between the temperature-induced A and B concentration changes and their respective absorbances (with respect to the reference temperature T_0) are

$$\begin{aligned} \mathrm{ABS}_{\lambda_1}(T) - \mathrm{ABS}_{\lambda_1}(T_0) &= \epsilon_A^{\lambda_1}([A]_T - [A]_{T_0}) \\ \mathrm{ABS}_{\lambda_2}(T) - \mathrm{ABS}_{\lambda_2}(T_0) &= \epsilon_A^{\lambda_2}([B]_T - [B]_{T_0}) \end{aligned} \quad (5)$$

However, for each amount of B (or A) that is formed by the action of temperature, an equal amount of A (or B) must be consumed, i.e.: $([A]_T - [A]_{T_0}) = -([B]_T - [B]_{T_0})$. Equation 5 then transforms into

$$\mathrm{ABS}_{\lambda_2}(T) = -\frac{\epsilon_B^{\lambda_2}}{\epsilon_A^{\lambda_1}}\mathrm{ABS}_{\lambda_1}(T) + \left[\frac{\epsilon_B^{\lambda_2}}{\epsilon_A^{\lambda_1}}\mathrm{ABS}_{\lambda_1}(T_0) + \mathrm{ABS}_{\lambda_2}(T_0)\right] \quad (6)$$

Thus, if the temperature has an effect on the A ↔ B equilibrium, a plot of $\mathrm{ABS}_{\lambda_2}(T)$ vs $\mathrm{ABS}_{\lambda_1}(T)$ must be a straight line with slope $-(\epsilon_B^{\lambda_2}/\epsilon_A^{\lambda_1})$ and the experimentally measured absorbance values are amenable to linear fitting (Figure 4). By this method, we determined the extinction

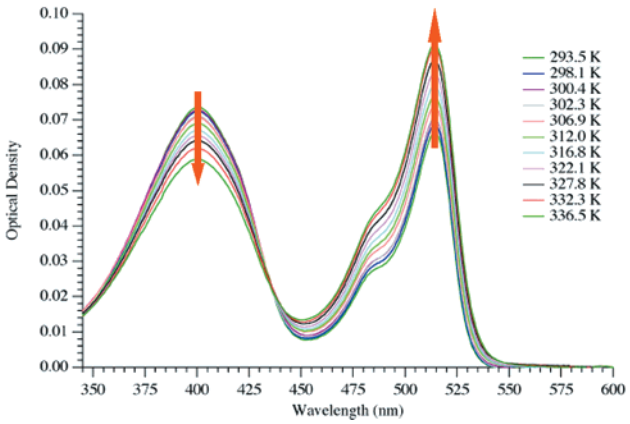

FIGURE 3: Temperature dependence of E^{2}GFP absorption spectrum in the 293.5−336.5 K range at pH ≫ p*K* (A ↔ B equilibrium active). Red arrows show increasing temperature.

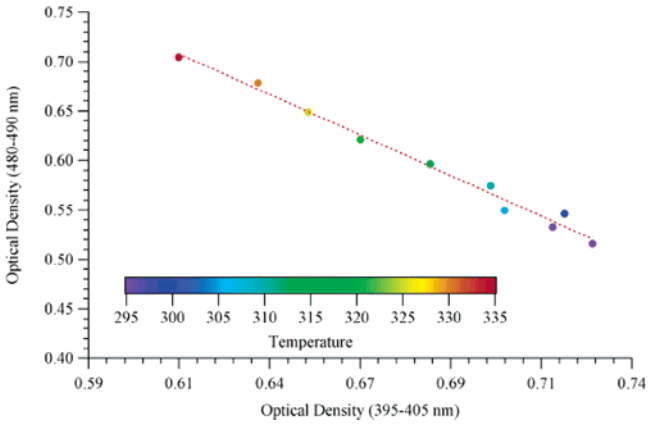

FIGURE 4: Absorbance of the B state vs absorbance of the A state of E^{2}GFP in the 295−335 K range at pH ≫ p*K*: the linear trend is the result of mass balance between these two states.

coefficient ratio ϵ_B/ϵ_A from the slope of the linear fit. Knowing ϵ_B/ϵ_A, the equilibrium constants of A ↔ B protonation exchange at different temperature could be calculated by

$$K_{AB}(T) = \frac{[B]_T}{[A]_T} = \left(\frac{ABS_{\lambda_2}(T)}{ABS_{\lambda_1}(T)}\right)\left(\frac{\epsilon_B^{\lambda_2}}{\epsilon_A^{\lambda_1}}\right)^{-1} \quad (7)$$

From the K_{AB} values, we found that at high pH and 296 K the A state is much more populated than the B state in E^{1}GFP (A, 94%; B, 6%) and E^{2}GFP (A, 61%; B, 29%), whereas the opposite pattern holds for EGFP (A, 16%; B, 84%). The A and B relative populations in EGFP are very similar to the fluorescence correlation spectroscopy (FCS[1]) bright (88%) and dark (12%) fractions determined for the same mutant at high pH and 488 nm excitation (*31*). At this wavelength, A and B have a large difference in molar fluorescence emission, and FCS-based calculations should indeed afford the relative populations of the two states. Consistently, FCS analysis of the "super folder" GFP (SFGFP), a mutant closely related to EGFP, showed the existence of an excitation-independent dark fraction that decreases with pH down to an asymptotic value around 15−20% for pH > 8 (*32*). By combining K_{AB} and $K_{A'M}$ into eq 3, the microscopic dissociation constants of ChroH ($K_{A'B}$) and XH ($K_{A'A}$) of E^{n}GFPs were calculated (Table 1).

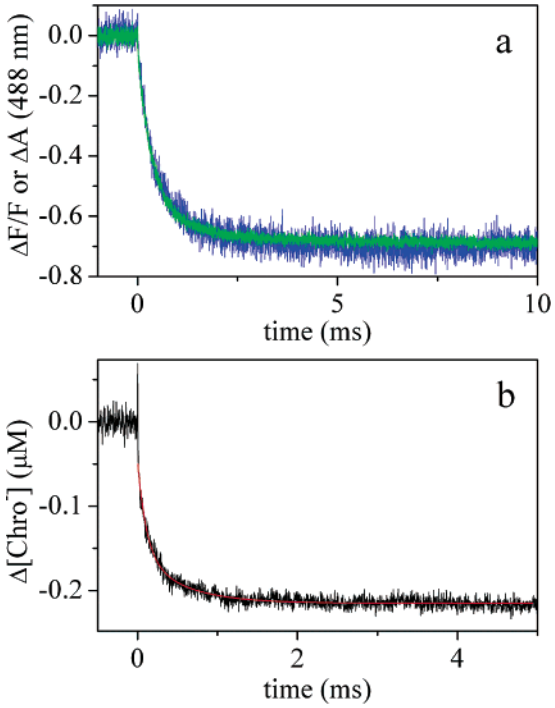

FIGURE 5: (a) Changes in absorbance at 488 nm (blue) and in the fluorescence emission (green) following a single 355 nm, 10 mJ laser pulse for an aqueous solution containing 2-NBA (2 mM) and EGFP. Absorbance changes were normalized to the relative fluorescence changes to show the perfect overlap of the two curves. (b) Time courses of changes in chromophore concentration (black) of E^{2}GFP together with fitting line (red line). Prepulse pH was about 8, corresponding to an increase in effective free proton concentration of about 95 μM.

For Mut2 variants, the slight changes in the absorption spectra could not be correlated to any definite trend (not shown). One could attribute the lack of temperature sensitivity of the A ↔ B equilibrium in the Mut2 class to a common enthalpy change close to zero. It seems very unlikely, however, that the enthalpy of XH deprotonation compensates exactly that of chromophore protonation for an entire class of mutants. Furthermore, enthalpic differences as small as 0.5 kcal/mol could be determined by our method for the A′ ↔ M equilibrium (data not shown). A much more convincing hypothesis is that the A state is not populated at high pH and room temperature (RT) in Mut2 derivatives, as witnessed also by the absorption spectrum of the M state, where the signal of neutral chromophore is nearly absent. Accordingly, we assume that for Mut2s the M state identifies with B, and we set $K_{A'M} = K_{A'B}$ (Table 1).

Kinetics of GFP Protonation. We exploited the photoinduced acidification of the solution, obtained by photoexcitation of aqueous 2-nitrobenzaldehyde (2-NBA), to shift the equilibrium between the ground states of EGFP, E^{1}GFP, E^{2}GFP, and Mut2Y. The kinetic characteristics of the other mutants were previously reported by some of us (*22*).

As expected, absorbance and fluorescence signals exhibit the same kinetic behavior (Figure 5a), displaying changes on the micro- to millisecond time scale. The kinetic traces were interpreted by using a reaction scheme similar to that previously reported by us for Mut2 variants (*22*), taking into account all the ionizable residues in the protein. The ionizable residues exposed to the solvent are organized in two groups according to their chemical function (carboxylic acid,

RCOOH, and imidazole, His), and the average contribution of each group was considered for the interpretation of the kinetic data. The ionizable side chains of Lys and Tyr residues are completely protonated at the prepulse pH of the kinetic experiments (pH = 8) and do not contribute to the overall proton-transfer equilibria. Conversely, the protonation reactions of ChroH and the XH site are considered in detail according to the features of the 2S model (Scheme 1).

The numerical fitting of the relaxation kinetics (a sample fit for E^{2}GFP is given in Figure 5b) allows us to estimate the microscopic rate constants as well as the dissociation pK values of ChroH and XH (Table 1). Remarkably and for all proteins, the kinetic p$K_{A'B}$ were found in excellent agreement with the corresponding equilibrium values obtained from steady-state measurements. Excellent agreement was displayed also between equilibrium and kinetic p$K_{A'A}$ values within the E^{n}GFP class.

The rate constants of chromophore direct protonation (k_1) are rather low if compared with the values reported for proton binding to solvent exposed protonatable sites on proteins ($\approx 10^{10}$ M^{-1} s^{-1}) (*33*), indicating a mediated pathway of proton entry (*22*). k_1 follows the trend Mut2G (10^8) $\gg$ EGFP $\sim$ E^{1}GFP $\sim$ E^{2}GFP $\sim$ Mut2Y (10^7) $\gg$ Mut2 (10^6) $\gg$ Mut2V (10^5), thus suggesting a large effect of the mutation pattern on the chromophore solvent accessibility. By FCS, a much higher value (1.53×10^9 M^{-1}s^{-1}) was found for the EGFP chromophore protonation rate constant (*31*). FCS monitors the fluorescence fluctuations of the chromophore protonation state, however, and this rate constant may reflect the fast shuttling between ChroH and a molecule capable of relaying the proton from the external buffer, rather than the direct protonation of the chromophore. By using a laser pH-jump method, a pH-dependent kinetic rate constant for EGFP chromophore protonation falling in the $(0.5-3.5) \times 10^8$ M^{-1} s^{-1} range was reported (*34*). The different experimental layout and kinetic analysis based on a much simpler protonation scheme hinders a quantitative comparison with our data.

Proton binding rate to carboxylates (k_4) and to histidines (k_7) is in agreement with data reported in the literature (*35*, *36*). Exchange rate constants were not determined with high precision, as they have a minor contribution to the observed kinetics. Tabulated data indicate slow exchange between surface proton acceptors and ChroH (k_{-5}, k_9) and suggest that the associated proton-transfer processes are not very efficient (*33*, *37*). In E^{n}GFPs, the XH residue seems to shuttle the proton to the chromophore (k_{-3}) with low efficiency, contrary to Mut2 variants. Consistently with the highest acidity of the XH residue, E^{1}GFP displayed also the highest value of k_{-3}.

Significantly, the fitting procedure on EGFP data was much improved by assuming that the proton binding process involves a millisecond monoexponential decay independent of the pH-jump (k_c). This finding, already reported for Mut2, Mut2V, and Mut2G (*22*), likely indicates the presence of a slow conformational change triggered by pH decrease.

Structural Analysis of E^{2}GFP at High pH. The 1.8 Å resolution crystal structure of E^{2}GFP was determined collecting data at room temperature (298 K) from a crystal grown at pH 9.0. The structure revealed the presence of two conformational states (Figure 6). These differ mainly in the chromophore region, while the β-barrel motif typical of GFP

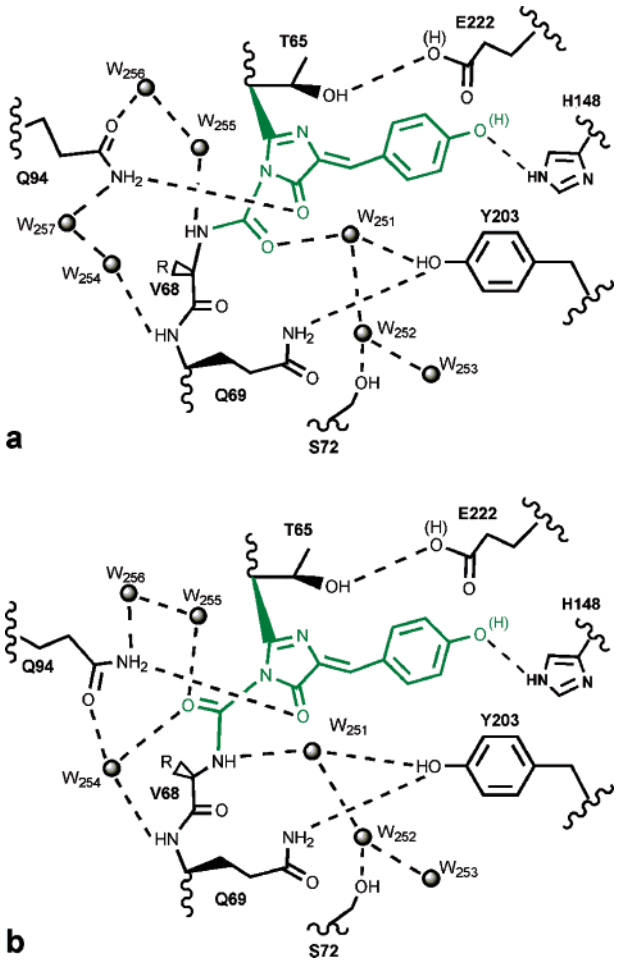

FIGURE 6: (a) Closed and (b) open conformation of E^{2}GFP, showing conformational changes and hydrogen bonding pattern around the chromophore (green).

was virtually unchanged. The more populated of these states (occupancy index: 70%) was characterized by a torsion angle N3−CA3−C3−V68 N joining the chromophore to the protein backbone around 173°, and the chromophore atom O3 pointed internally toward Y203 (we label this "closed" conformation, Figure 6a). Conversely, in the less populated conformational state (occupancy index: 30%) the value of the torsion angle N3−CA3−C3−V68 N is −30°. As a consequence, the chromophore atom O3 points externally toward Q94 ("open" conformation, Figure 6b), in agreement with the GFP structures reported so far. The O3 peptide bond flipping leads to an adjustment of Q94 side chain position and to an extended change in the H-bond network around the chromophore. Interestingly, E^{2}GFP assumes the same "open" conformation in the presence of bound negatively charged chloride ions (D. Arosio, in press).

DISCUSSION

Relevance of Two-Ionizable Sites for the Optical Properties of GFP Mutants. Different protonation states of the chromophore are invoked to rationalize the main photophysical properties of wtGFP and many of its mutants. This should not lead to the conclusion that the chromophore phenol (ChroH) is the only protonatable site relevant to GFP optical properties. Indeed, inclusion of the chromophore ionization states alone cannot provide a rational explanation of the phenomenology observed for several GFP mutants.

Examples of open questions are the presence of the neutral-chromophore optical band at high pH (*14*−*17*) and the pH-dependence of the dissociation constant calculated by thermal analysis (*18*).

In this work we investigate the possible existence and impact of a second protonation site (XH) adjacent to ChroH. This concept was first proposed by Webb et al. on the basis of FCS measurements (*17*, *31*) and by Scharnagl et al. from theoretical calculations (*38*). Interestingly, a second protonation site was recently proposed to contribute to the optical properties of the cmFP512 fluorescent protein from *Cerianthus membranaceus* (*39*).

Inclusion of the ionization of this hypothetical second protonation site leads us to consider four distinct ground states, A′ (ChroH and XH), A (ChroH and X^-), B ($Chro^-$ and XH), and B′ ($Chro^-$ and X^-) (2S model, see Scheme 1). Furthermore, XH can be thermodynamically coupled to ChroH, i.e., the ionization of the XH residue may affect the free energy of ChroH ionization and vice versa. Such a complex configuration may appear to be inconsistent with a large body of spectroscopic investigations and even our own data of Figure 1. One must realize, however, that a molecule governed by a two-site protonation scheme exhibits a phenomenology characteristic of a simple single-site equilibrium in two different thermodynamic regimes.

First, let us consider the B′ state that corresponds to complete deprotonation of ChroH and XH. If these two sites are strongly anti-cooperatively coupled (i.e., deprotonation of one inhibits deprotonation of the other), B′ may not be populated in the stability pH range of the protein. Accordingly, the optical response would follow an apparent single-site equilibrium between the fully protonated state A′ and a mixed form M of the A and B states until unfolding (Scheme 2). Thus, the 2S model explains why the band of the neutral chromophore persists at high pH up to unfolding pH. On the contrary, as mentioned above, the latter fact is not explained within a single-ionization site scheme. The second regime occurs when XH and ChroH are uncoupled. In this case, the optical properties of the protein follow the single-ionization equilibrium of ChroH, i.e., the apparent M state in Scheme 2 identifies with B.

To better characterize these two regimes, we focused our studies on two GFP families, E^{n}GFPs and Mut2s, which display paradigmatically opposite optical responses upon pH changes. Concerning E^{n}GFPs, we showed that E^{1}GFP and E^{2}GFP mutants display a large constant absorption band peaked at 400 nm above pH 8. For EGFP, absorption of the neutral chromophore is just a shoulder of the large anionic peak when the proton concentration is low (Figure 2), but thermal analysis showed that the fractional population of the A state is around 16% at high pH. This figure is in excellent agreement with the dark-fraction value determined by FCS at pH 9 by Schwille for the same mutant (*31*) and by Cotlet for the super folder GFP, a variant closely related to EGFP (*32*). These results indicate that strongly anti-cooperative thermodynamic coupling between the two sites is a common feature of E^{n}GFPs. Here, the general validity of the 2S model is also confirmed by the remarkable similarity of the p*K* values of ChroH and XH determined by both the equilibrium and kinetic experiments (Table 1).

The absence of neutral chromophore absorption at high pH and the lack of thermally induced shift of chromophore population suggest that ChroH and XH are not thermodynamically coupled in Mut2s. Furthermore, the experimental p*K* determined from steady-state experiments (p$K_{A'M}$) is larger than the kinetically found p$K_{A'A}$. As witnessed by eq 3, this situation is not compatible with the regime where ChroH and XH are coupled.

Nature of the Second Ionizable Site (XH). The existence of a second ionizable site around the chromophore prompts for its identification. Inspection of the GFP structure shows that only two residues are close enough to the chromophore and ionizable in the stability range of the protein: H148 and E222. We recently discussed the role of H148 as a proton gate between solution and chromophore region in Mut2s by means of kinetic relaxation experiments (*22*). H148 stands as the most likely candidate for the proton relay role, in light of available experimental findings (*40*) and molecular dynamic simulations (*41*).

We propose to identify X = H148 for this mutant class. Under this hypothesis H148 is not coupled to ChroH. This hypothesis is consistent with our suggestion that anti-cooperative coupling is generated by the concomitant presence of two negative charges in close proximity: one on the chromophore phenolate and one on the XH residue in anionic form. Indeed, the second ionization p*K* of histidine lateral chain is so high that the presence of a negative charge on the imidazole ring is unlikely in the pH stability range of the protein.

A different scenario applies to E^{n}GFPs. In this case the best candidate for the role of second proton binding site is glutamate 222. The proton donor/acceptor characteristic of E222 was widely invoked for the ESPT mechanism of wtGFP (*8*), and strong interactions between the chromophore and E222 were calculated for wtGFP and a series of mutants in ref *38*. Remarkably, the high-pH absorption spectra of EGFP and EGFP/E222Q reported in a recent study clearly show the absence of the neutral chromophore band (i.e., the A state) in the E222Q mutant (*2*). In the same study, an E222 dissociation p*K* around 6.5 was estimated from EGFP folding kinetics in excellent agreement with the p$K_{A'A}$ we found for this protein (Table 1) (*2*). Even more strikingly the additional E222Q substitution in T203Y completely abolishes the absorption of the A state at pH 10, though the chromophore is overwhelmingly neutral at high pH in T203Y (*42*) and the closely related E^{1}GFP mutant (Figure 7). If we attribute the same ϵ_{UV} at 278 nm to E^{1}GFP (F64L/T203Y) and T203Y/E222Q, we obtain a molar extinction coefficient of the anionic chromophore in T203Y/E222Q around 56,300 cm^{-1} M^{-1} at 509 nm. By using this value as an estimate for the intrinsic absorption of the B state in T203Y E^{n}GFPs mutants, we determined a B-state fraction of 8.9% in E^{1}GFP and 39.5% in E^{2}GFP, in good agreement with our previous results.

E^{2}GFP is a good candidate for a structural analysis of the configurations associated with the different protonation states. Our X-ray analysis of E^{2}GFP at pH 9 did indicate the presence of two different structural arrangements of the chromophore and its immediate environment, which were labeled "closed" (Figure 6a) and "open" (Figure 6b) conformations. This is further support to the existence of two protonation ground states at high pH for this mutant. Spectroscopic data and molecular dynamics simulations, which will be reported elsewhere, confirm that the E222

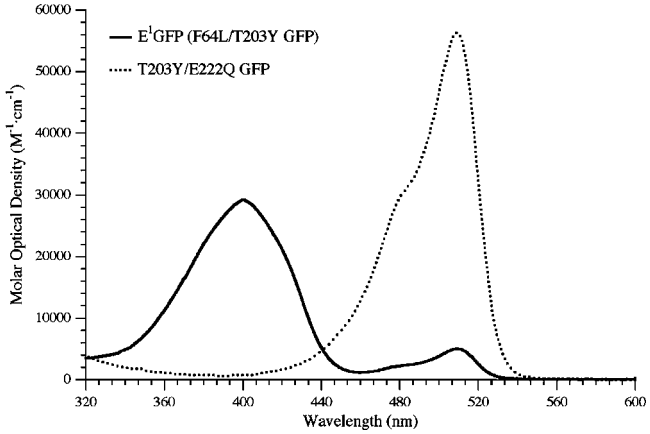

FIGURE 7: Comparison between the molar absorption spectra of E¹GFP and T203Y/E222Q GFP at high pH. Absorption spectra of T203Y/E222Q GFP at pH 10 was kindly provided by Prof. Gregor Jung and has been published in ref *42*. For T203Y/E222Q we set the extinction coefficients at 278 nm (ϵ_{UV}) at 31,350 (M^{-1} cm^{-1}), analogous to E¹GFP.

ionization state is associated with the conformational change: the A state corresponds to the "open" configuration, while the "closed" one is associated with A′ and B states only. We believe that the discrepancy between the occupancy indexes and the population of A and B can be attributed to the different physical state of the protein (crystal structure vs solution).

His148 in E²GFP structure does not change its configuration between "open" and "closed" forms, and it is at hydrogen-bonding distance to the chromophore (Figure 6). In addition, its position is superimposable to that of the same residue in many other GFP mutants such as wtGFP [pdb code: 1GFL (*43*)] and YFP [pdb code: 2YFP (*30*)]. It is likely that also in E^{n}GFPs H148 plays the same proton gate role between the external buffer and ChroH as demonstrated for Mut2s. Vice versa, the position of E222 makes this residue an unlikely proton "gate" able to open a transient channel for H^+ ions from the bulk to the shielded chromophore. This is consistent with the much lower rate for proton transfer from XH to the chromophore in E^{n}GFPs with respect to Mut2s. We conclude that in E^{n}GFPs XH = E222.

Remarkably, analysis of p$K_{A'A}$ and p$K_{A'B}$ values in E^n-GFPs indicates that the S65T and T203Y replacements inhibit XH and CroH ionizations, respectively (Table 1). We believe that these effects are related to the well-known hydrogen-bonding stabilization of anionic E222 by S65 (*13*, *44*) and of the chromophore phenolate by T203 (*8*, *13*).

E222 Ionization and Ground States of Other GFPs. On account of the generality of the 2S model, we believe that E222 ionization must play a pivotal role in determining the ground-state configurations of other GFP variants. Photoactivatable GFP (T203H GFP) is a remarkable GFP mutant whose fluorescence can be enhanced up to 100 times upon irradiation at 350−410 nm (*45*). Before irradiation and at pH ≫ p*K* (p*K* is around 5.0, see Supporting Information of ref *45*), T203H GFP shows predominant neutral absorption around 400 nm with low fluorescence. After irradiation, the absorption spectrum displays significant absorption of the anionic form of the chromophore, which fluoresces strongly. Analogously to what happens in wtGFP, UV-driven E222 decarboxylation is supposed to be responsible for T203H GFP photoconversion (*45*). The 2S model provides a rational base for the observed optical behavior: glutamate loss leads to uncoupling with ChroH, thereby shifting the internal equilibrium at high pH from the A state (predominant prior to irradiation) to the B state (predominant after irradiation).

A further example is provided by YFP (S65G/V68L/S72A/T203Y GFP). YFP is a popular yellow GFP mutant that displays pH-dependent optical behavior similar to Mut2Y, to which it is structurally akin. Thus, no neutral chromophore band can be seen in the absorption spectrum when the pH is raised well above p*K* (pK = 5.4) (*29*). The X-ray structure of YFP at pH 6.9 shows that the entire chromophore ring system of YFP has moved out toward the protein surface by about 0.9 Å in comparison to that of wtGFP, leading to a close approach between E222 and the chromophore imidazolinone ring nitrogen (2.7 Å instead of 4.3 Å for wtGFP), which are hydrogen-bonded to each other (*30*). Replacement of S65 with glycine subtracts a hydrogen-bond donor to anionic E222, forcing the glutamic residue in the neutral form. Likewise T65 is known to inhibit E222 ionization in S65T GFP (*13*). The existence of a strong hydrogen bond between E222 and the imidazolinone ring nitrogen is likely to further inhibit E222 ionization. Taken together these two effects may lead to decoupling the protonation equilibria of E222 and ChroH, thus rationalizing the pH-dependent optical characteristics of YFP.

Conclusions. In conclusion, due to experimental evidence that cannot be rationalized on the basis of the single ionization equilibrium of the chromophore, we proposed a general model of GFP protonation comprising two ionization sites. The presence of some ionizable residues around the chromophore was demonstrated by the first X-ray analyses of GFPs (*8*), yet internal proton exchanges were considered only in few photophysical studies so far. Our model can account for the reported optical behavior of different GFP mutants since it applies either when the residues are thermodynamically coupled or when they are independent. Only in the latter case the optical properties depend solely on the chromophore ionization.

We believe that the origin of the paradigmatic protonation regimes described here must be searched in significant differences of the chromophore environment triggered by subtle changes in the mutation patterns. Interestingly, the X-ray structure of E²GFP shows that E222 and the chromophore imidazolinone ring nitrogen are separated by 4.2 Å, too far to be hydrogen-bonded. deGFP1, a GFP mutant with predominance of neutral chromophore at high pH, is characterized by a similar distance of 4.38 Å. Presumably, the distance between E222 and the chromophore imidazolinone is a crucial parameter for the thermodynamic coupling of ChroH and the glutamate in position 222. Also, serine replacement in position 65 with non-protic amino acids prevents the stabilization of anionic E222 by removing its hydrogen bond with S65. In Mut2s, the latter mechanism was invoked to explain the found pH-dependent optical properties. Further experiments to elucidate these aspects are under way.

ACKNOWLEDGMENT

We thank Prof. Gregor Jung for kindly providing the T203Y/E222Q absorption spectrum at pH 10. We also thank

Dr. Valentina Tozzini for stimulating discussions and Dr. Samanta Raboni for preparing the Mut2 GFP variants.

SUPPORTING INFORMATION AVAILABLE

Crystallographic data collection parameters and refinement statistics of E^2GFP and the theoretical description of the augmented component analysis method. This material is available free of charge via the Internet at http://pubs.acs.org.

REFERENCES

1. Shaner, N. C., Steinbach, P. A., and Tsien, R. Y. (2005) A guide to choosing fluorescent proteins, *Nat. Methods 2*, 905−9.
2. Sniegowski, J. A., Lappe, J. W., Patel, H. N., Huffman, H. A., and Wachter, R. M. (2005) Base catalysis of chromophore formation in Arg96 and Glu222 variants of green fluorescent protein, *J. Biol. Chem. 280*, 26248−55.
3. Niwa, H., Inouye, S., Hirano, T., Matsuno, T., Kojima, S., Kubota, M., Ohashi, M., and Tsuji, F. I. (1996) Chemical nature of the light emitter of the Aequorea green fluorescent protein, *Proc. Natl. Acad. Sci. U.S.A. 93*, 13617−22.
4. Zhang, J., Campbell, R. E., Ting, A. Y., and Tsien, R. Y. (2002) Creating new fluorescent probes for cell biology, *Nat. Rev. Mol. Cell. Biol. 3*, 906−18.
5. Chattoraj, M., King, B. A., Bublitz, G. U., and Boxer, S. G. (1996) Ultra-fast excited state dynamics in green fluorescent protein: multiple states and proton transfer, *Proc. Natl. Acad. Sci. U.S.A. 93*, 8362−7.
6. Cinelli, R. A. G., Tozzini, V., Pellegrini, V., Beltram, F., Cerullo, G., Zavelani-Rossi, M., De, Silvestri, S., Tyagi, M., and Giacca, M. (2001) Coherent dynamics of photoexcited green fluorescent proteins, *Phys. Rev. Lett. 86*, 3439−3442.
7. McAnaney, T. B., Park, E. S., Hanson, G. T., Remington, S. J., and Boxer, S. G. (2002) Green fluorescent protein variants as ratiometric dual emission pH sensors. 2. Excited-state dynamics, *Biochemistry 41*, 15489−94.
8. Brejc, K., Sixma, T. K., Kitts, P. A., Kain, S. R., Tsien, R. Y., Ormo, M., and Remington, S. J. (1997) Structural basis for dual excitation and photoisomerization of the Aequorea victoria green fluorescent protein, *Proc. Natl. Acad. Sci. U.S.A. 94*, 2306−11.
9. Lossau, H., Kummer, A., Heinecke, R., PollingerDammer, F., Kompa, C., Bieser, G., Jonsson, T., Silva, C. M., Yang, M. M., Youvan, D. C., and MichelBeyerle, M. E. (1996) Time-resolved spectroscopy of wild-type and mutant Green Fluorescent Proteins reveals excited state deprotonation consistent with fluorophore-protein interactions, *Chem. Phys. 213*, 1−16.
10. Kennis, J. T., Larsen, D. S., van Stokkum, I. H., Vengris, M., van Thor, J. J., and van Grondelle, R. (2004) Uncovering the hidden ground state of green fluorescent protein, *Proc. Natl. Acad. Sci. U.S.A. 101*, 17988−93.
11. Kneen, M., Farinas, J., Li, Y., and Verkman, A. S. (1998) Green fluorescent protein as a noninvasive intracellular pH indicator, *Biophys. J. 74*, 1591−9.
12. Llopis, J., McCaffery, J. M., Miyawaki, A., Farquhar, M. G., and Tsien, R. Y. (1998) Measurement of cytosolic, mitochondrial, and Golgi pH in single living cells with green fluorescent proteins, *Proc. Natl. Acad. Sci. U.S.A. 95*, 6803−8.
13. Elsliger, M. A., Wachter, R. M., Hanson, G. T., Kallio, K., and Remington, S. J. (1999) Structural and spectral response of green fluorescent protein variants to changes in pH, *Biochemistry 38*, 5296−301.
14. Hanson, G. T., McAnaney, T. B., Park, E. S., Rendell, M. E., Yarbrough, D. K., Chu, S., Xi, L., Boxer, S. G., Montrose, M. H., and Remington, S. J. (2002) Green fluorescent protein variants as ratiometric dual emission pH sensors. 1. Structural characterization and preliminary application, *Biochemistry 41*, 15477−88.
15. Kummer, A. D., Wiehler, J., Rehaber, H., Kompa, C., Steipe, B., and Michel-Beyerle, M. E. (2000) Effects of threonine 203 replacements on excited-state dynamics and fluorescence properties of the green fluorescent protein (GFP), *J. Phys. Chem. B 104*, 4791−4798.
16. Jung, G., Wiehler, J., and Zumbusch, A. (2005) The photophysics of green fluorescent protein: influence of the key amino acids at positions 65, 203, and 222, *Biophys. J. 88*, 1932−47.
17. Hess, S. T., Heikal, A. A., and Webb, W. W. (2004) Fluorescence photoconversion kinetics in novel green fluorescent protein pH sensors (pHluorins), *J. Phys. Chem. B 108*, 10138−10148.
18. McAnaney, T. B., Shi, X. H., Abbyad, P., Jung, H., Remington, S. J., and Boxer, S. G. (2005) Green fluorescent protein variants as ratiometric dual emission pH sensors. 3. Temperature dependence of proton transfer, *Biochemistry 44*, 8701−8711.
19. Bizzarri, R., Arcangeli, C., Arosio, D., Ricci, F., Faraci, P., Cardarelli, F., and Beltram, F. (2006) Development of a novel GFP-based ratiometric excitation and emission pH indicator for intracellular studies, *Biophys. J. 90*, 3300−14.
20. Patterson, G. H., Knobel, S. M., Sharif, W. D., Kain, S. R., and Piston, D. W. (1997) Use of the green fluorescent protein and its mutants in quantitative fluorescence microscopy, *Biophys. J. 73*, 2782−90.
21. Cormack, B. P., Valdivia, R. H., and Falkow, S. (1996) FACS-optimized mutants of the green fluorescent protein (GFP), *Gene 173*, 33−8.
22. Abbruzzetti, S., Grandi, E., Viappiani, C., Bologna, S., Campanini, B., Raboni, S., Bettati, S., and Mozzarelli, A. (2005) Kinetics of acid-induced spectral changes in the GFPmut2 chromophore, *J. Am. Chem. Soc. 127*, 626−35.
23. van Thor, J. J., Gensch, T., Hellingwerf, K. J., and Johnson, L. N. (2002) Phototransformation of green fluorescent protein with UV and visible light leads to decarboxylation of glutamate 222, *Nat. Struct. Biol. 9*, 37−41.
24. Cinelli, R. A. G., Pellegrini, V., Ferrari, A., Faraci, P., Nifosi, R., Tyagi, M., Giacca, M., and Beltram, F. (2001) Green fluorescent proteins as optically controllable elements in bioelectronics, *Appl. Phys. Lett. 79*, 3353−3355.
25. Nifosi, R., Ferrari, A., Arcangeli, C., Tozzini, V., Pellegrini, V., and Beltram, F. (2003) Photoreversible dark state in a tristable green fluorescent protein variant, *J. Phys. Chem. B 107*, 1679−1684.
26. Leslie, A. G. W. (1991) in *Cristallographic Computing* (Moras, D., Podjarni, A. D., and Thierry, J. C., Eds.) pp 50−61, Oxford University Press, Oxford, U.K.
27. Ullmann, G. M. (2003) Relations between protonation constants and titration curves in polyprotic acids: A critical view, *J. Phys. Chem. B 107*, 1263−1271.
28. Ward, W. W., and Bokman, S. H. (1982) Reversible denaturation of Aequorea green-fluorescent protein: physical separation and characterization of the renatured protein, *Biochemistry 21*, 4535−40.
29. Wachter, R. M., Yarbrough, D., Kallio, K., and Remington, S. J. (2000) Crystallographic and energetic analysis of binding of selected anions to the yellow variants of green fluorescent protein, *J. Mol. Biol. 301*, 157−71.
30. Wachter, R. M., Elsliger, M. A., Kallio, K., Hanson, G. T., and Remington, S. J. (1998) Structural basis of spectral shifts in the yellow-emission variants of green fluorescent protein, *Structure 6*, 1267−77.
31. Haupts, U., Maiti, S., Schwille, P., and Webb, W. W. (1998) Dynamics of fluorescence fluctuations in green fluorescent protein observed by fluorescence correlation spectroscopy, *Proc. Natl. Acad. Sci. U.S.A. 95*, 13573−8.
32. Cotlet, M., Goodwin, P. M., Waldo, G. S., and Werner, J. H. (2006) A comparison of the fluorescence dynamics of single molecules of a green fluorescent protein: one- versus two-photon excitation, *ChemPhysChem 7*, 250−60.
33. Gutman, M., and Nachliel, E. (1997) Time-resolved dynamics of proton transfer in proteinous systems, *Annu. Rev. Phys. Chem. 48*, 329−56.
34. Saxena, A. M., Udgaonkar, J. B., and Krishnamoorthy, G. (2005) Protein dynamics control proton transfer from bulk solvent to protein interior: A case study with a green fluorescent protein, *Protein Sci. 14*, 1787−1799.
35. Abbruzzetti, S., Viappiani, C., Small, J. R., Libertini, L. J., and Small, E. W. (2000) Kinetics of local helix formation in poly-L-glutamic acid studied by time-resolved photoacoustics: Neutralization reactions of carboxylates in aqueous solutions and their relevance to the problem of protein folding, *Biophys. J. 79*, 2714−2721.
36. Gutman, M., and Nachliel, E. (1990) The Dynamic Aspects of Proton-Transfer Processes, *Biochim. Biophys. Acta 1015*, 391−414.
37. Yam, R., Nachliel, E., and Gutman, M. (1988) Time-Resolved Proton Protein-Interaction - Methodology and Kinetic-Analysis, *J. Am. Chem. Soc. 110*, 2636−2640.

38. Scharnagl, C., Raupp-Kossmann, R., and Fischer, S. F. (1999) Molecular basis for pH sensitivity and proton transfer in green fluorescent protein: Protonation and conformational substates from electrostatic calculations, *Biophys. J. 77*, 1839−1857.
39. Nienhaus, K., Renzi, F., Vallone, B., Wiedenmann, J., and Nienhaus, G. U. (2006) Exploring chromophore−protein interactions in fluorescent protein cmFP512 from Cerianthus membranaceus: X-ray structure analysis and optical spectroscopy, *Biochemistry 45*, 12942−53.
40. Seifert, M. H., Georgescu, J., Ksiazek, D., Smialowski, P., Rehm, T., Steipe, B., and Holak, T. A. (2003) Backbone dynamics of green fluorescent protein and the effect of histidine 148 substitution, *Biochemistry 42*, 2500−12.
41. Helms, V., Straatsma, T. P., and McCammon, J. A. (1999) Internal dynamics of green fluorescent protein, *J. Phys. Chem. B 103*, 3263−3269.
42. Jung, G., and Zumbusch, A. (2006) Improving autofluorescent proteins: comparative studies of the effective brightness of Green Fluorescent Protein (GFP) mutants, *Microsc. Res. Tech. 69*, 175−85.
43. Yang, F., Moss, L. G., and Phillips, G. N., Jr. (1996) The molecular structure of green fluorescent protein, *Nat. Biotechnol. 14*, 1246−51.
44. Nifosi, R., and Tozzini, V. (2003) Molecular dynamics simulations of enhanced green fluorescent proteins: effects of F64L, S65T and T203Y mutations on the ground-state proton equilibria, *Proteins 51*, 378−89.
45. Patterson, G. H., and Lippincott-Schwartz, J. (2002) A photoactivatable GFP for selective photolabeling of proteins and cells, *Science 297*, 1873−7.

BI602646R